JMEPEG (2012) 21:2600–2606
DOI: 10.1007/s11665-012-0267-3

1059-9495/$19.00

Hydrothermal Growth Mechanism of Controllable Hydrophilic Titanate Nanostructures on Medical NiTi Shape Memory Alloy

X. Rao, C.L. Chu, C.Y. Chung, and Paul K. Chu

(Submitted February 17, 2012; in revised form April 19, 2012)

Different titanate nanostructures were deposited on the surface of NiTi by a hydrothermal process using 5-20 M NaOH at 90-150 °C for 6-72 h. SEM and XRD analyses revealed that different structures such as nanoflakes, nanorods, nanograins, nanofibers, microwhiskers, etc., were formed. As the processing time was increased, the nanoflakes evolve into nanofibers or microwhiskers. Compared with pristine NiTi, the new surfaces displayed different degrees of hydrophilicity. A formation mechanism adopting the growth unit model of anion coordination-polyhedra is proposed. The general formation of titanate nanostructures can be visualized as a sequence of nucleation, formation, and combination of the growth units. The excellent controllability of this process with precise accuracy offers incredible potential in the surface modification of NiTi biomedical materials for medical applications.

Keywords biomaterials, modification, surface engineering

1. Introduction

Titanium and its alloy are frequently used in orthopedic implants and bone replacements because of their excellent mechanical strength, high chemical stability, and attractive biocompatibility. In particular, NiTi alloys with shape memory and superelastic properties are widely used in clinic applications (Ref 1). However, release of Ni from NiTi SMA due to its high Ni contents can cause allergenic and toxic reactions. Moreover, NiTi shape SMA has the tendency to corrode in the physiological environment thereby accelerating this release. Hence, it is necessary to improve the corrosion resistance of NiTi to mitigate Ni release to gain wider acceptance in the biomedical field (Ref 2-4). Nanostructures have recently been reported to have a significant influence on cell adhesion and proliferation (Ref 5-8). For instance, sodium titanate nanostructures not only exhibit good biocompatibility but also induce the formation of bone-like apatite (Ref 9-11). Present research indicates that it is a promising way to overcome the limitation of NiTi SMA in biomedical applications.

This article is an invited paper selected from presentations at the International Conference on Shape Memory and Superelastic Technologies 2011, held November 6-9, 2011, in Hong Kong, China, and has been expanded from the original presentation.

X. Rao and **C.L. Chu**, School of Materials Science and Engineering and Jiangsu Key Laboratory for Advanced Metallic Materials, Southeast University, Nanjing 211189, China; and **C.Y. Chung** and **Paul K. Chu**, Department of Physics & Materials Science, City University of Hong Kong, Tat Chee Avenue, Kowloon, Hong Kong, China. Contact e-mail: clchu@seu.edu.cn.

Low-temperature hydrothermal synthesis has attracted much attention due to the simple procedures and lower production costs. Most research activities have focused on the synthesis of dispersive sodium titanate using TiO_2 powders and alkaline media (Ref 12-18). Although the fabrication of sodium titanate on the NiTi is attracting more attention (Ref 19-22), the growth mechanism is relatively not well understood. In order to construct desirable NiTi surface to satisfy application demands, it is imperative to establish the growth mechanism that enables the controlled hydrothermal formation of sodium titanate on NiTi SMA.

In this work, various types of sodium titanate nanostructures are fabricated on NiTi by a hydrothermal process and the effects of the hydrothermal conditions including temperature, duration, and alkali concentration on the nanostructural characteristics are investigated. A mechanism for the formation of the controllable hydrophilic NiTi SMA surface (Ref 23) is also postulated.

2. Experimental Details

2.1 Preparation of Samples

A commercially available NiTi (50.8 at.% Ni) SMA plate for medical applications (Beijing Gee SMA Technology Co. Ltd, Beijing, China) with a martensite initiation temperature (M_s) of −12.8 °C and austenite finish temperature (A_f) of 33.4 °C was cut into small rectangular blocks with dimensions of 10 × 10 × 1 mm. The samples were chemically polished for several minutes using a solution of H_2O, HF, and HNO_3 with a 5:1:4 ratio. They were then ultrasonically washed in acetone for 10 min and deionized water for 10 min.

2.2 Experimental Design for Hydrothermal Synthesis

The orthogonal trial of L_{16} (4-5) was used to investigate the effect of three factors (temperature, duration, and alkali-concentration)

on sodium titanate nanostructure. As shown in Table 1, new hydrothermal conditions: 180 °C-72 h-10 M were used whereas the concentration of NaOH was fixed.

2.3 Microstructural Characterization

The morphology of the sodium titanate nanostructures on the NiTi SMA surfaces was examined by field-emission scanning electron microscopy (SEM, Sirion 2000, FEI Co., Denver, CO, USA) at 20 kV after the surfaces were coated with gold. X-ray diffraction (RAD IIA, Rigaku, Japan) with a Cr K_{α} source operated at 40 kV and 25 mA was used to determine the phase composition.

Table 1 Orthogonal test table

	Factors		
Levels	Concentration of NaOH, mol/L	Temperature, °C	Duration, h
1	5	90	6
2	10	120	12
3	15	150	44
4	20	180	72

2.4 Water Contact Angle Measurement

The samples were ultrasonically washed in acetone for 10 min and deionized water for 10 min, then dried at room temperature. The surface contact angles were measured using the liquid drop method on a contact angle goniometer (JC2000B, China). A 10 μL droplet of deionized water was put onto the sample surface to measure the contact angle. More than three samples were tested to obtain the average values along with the standard deviation.

3. Results

3.1 Sodium Titanate Nanostructures

Figure 1 depicts the SEM images of sodium titanate nanostructures fabricated by the hydrothermal reactions showing various types of sodium titanate nanostructures on the surface of NiTi SMA substrates for a fixed time duration. Short nanorod-like structures appear after hydrothermal treatment at 90 °C-6 h-5 M, as shown in Fig. 1(a). The features have diameters of 30-50 nm and lengths of 100-200 nm. With increasing temperature and concentration, the surface changes completely to a nanoflake-like structure (Fig. 1b) with heights

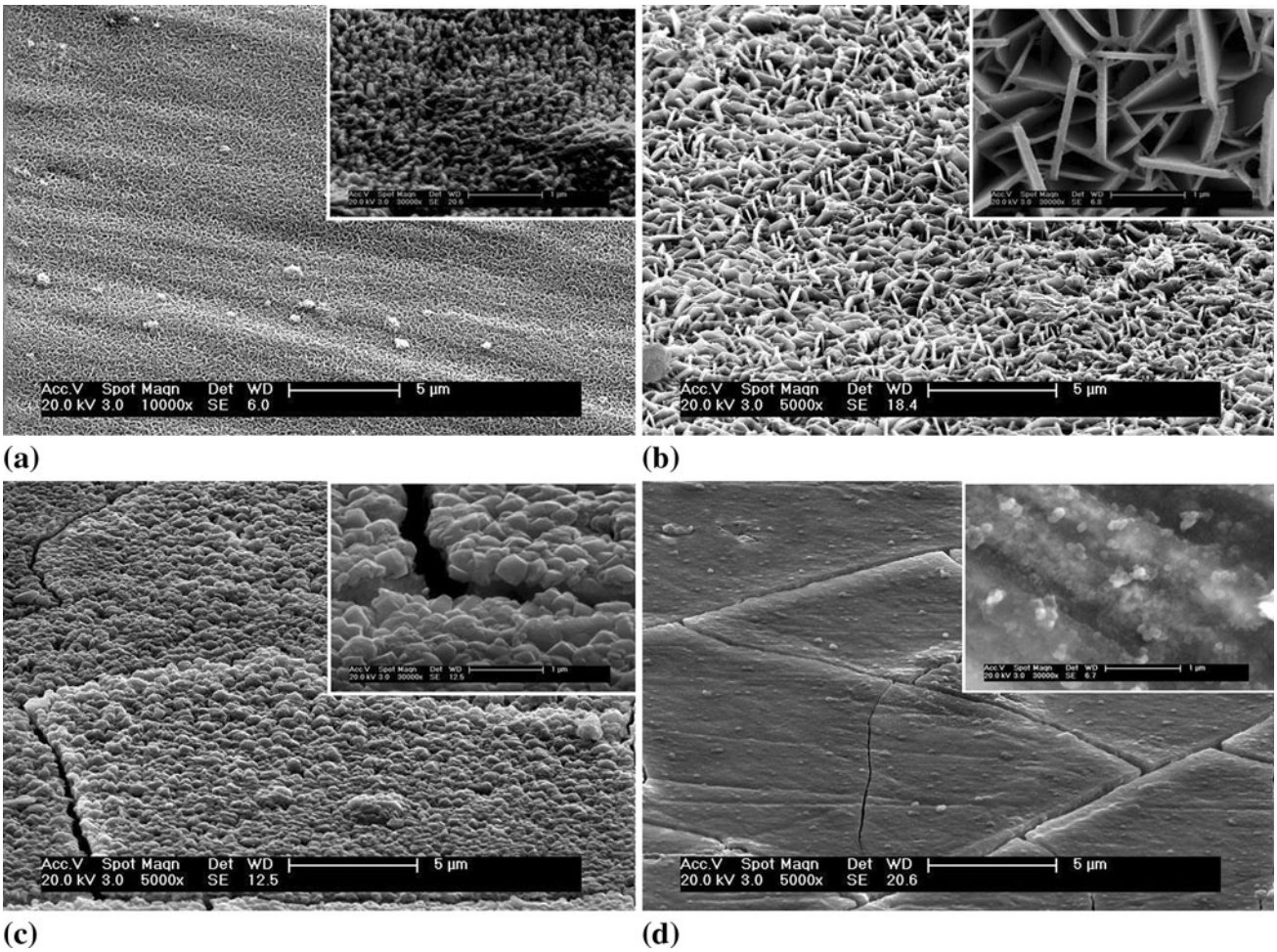

Fig. 1 Surface morphology of hydrothermally treated NiTi surface under different conditions. (a) 90 °C-6 h-5 M; (b) 120 °C-6 h-10 M; (c) 150 °C-6 h-15 M; and (d) 180 °C-6 h-20 M

of 200-600 nm, lengths of 0.5-1 μm, and widths of 80-120 nm. These nanoflake structures continue to transform into nanocube structures as the temperature and concentration reach 150 °C and 15 M, respectively. As shown in Fig. 1(c), the nanocube layer covers the substrate due to dehydration of titanates and cracks occur during the hydrothermal reaction. When the temperature and concentration are increased to 180 °C and 20 M, respectively, the nanostructures disappear and a compact sodium titanate layer covers the NiTi substrate, as shown in Fig. 1(d).

Figure 2 illustrates the transformation of the titanate nanostructures when the concentration is fixed. Compared with Fig. 1(b), as the temperature and time duration are increased to 150 °C and 72 h, respectively, nanoflake structures are replaced by nanorod structures. The nanorod structures can be found to have covered the entire surface (Fig. 2a, b). The average length of the titanate nanofibers is in the sub-millimeter range whereas the average diameter is on the nanometer scale. Haimin et al. (Ref 19) reported that titanate nanotubes were synthesized by hydrothermal treatment of metal titanium foil in 10 M NaOH solution at 150 °C for 2 h. At the same temperature and NaOH concentration, the titanate nanostructure exhibits a similar morphology for different durations. Hence, the time duration has little influence on the morphology of titanate structures at the early stage of the hydrothermal treatment. When the temperature reaches 180 °C, NiTi substrates are totally covered by sea urchin-like structure (Fig. 2c). The size of the titanate structures is observed to change from nanoscale to microscale, as shown in Fig. 2(d). The average length of the microwhiskers is several tens of micrometers and the average diameter is about 500 nm.

3.2 XRD and EDS Analyses

The XRD patterns of the product obtained by the reaction between titanium dioxide and aqueous sodium hydroxide are shown in Fig. 3 revealing complicated surface phase compositions including major $Na_4Ti_3O_8$ and minor NiTi, $Na_4Ti_5O_{12}$. Previous results show that the compositions of produced titanate are different due to various hydrothermal processing parameters such as temperature, time duration, and NaOH concentration (Ref 15, 19, 20, 22). $Na_2Ti_3O_7$, $Na_2Ti_2O_5$, $Na_2Ti_6O_{13}$ are the products shown in these reports. Yongjie et al. (Ref 24) have confirmed that $Na_4Ti_3O_8$ can also be fabricated by a hydrothermal process. The reaction $3TiO_2 + 4NaOH \rightarrow Na_4Ti_3O_8 + 2H_2O$ occurs when the NaOH solution and titanium oxide mass ratio is 4:1. Moreover, $Na_4Ti_3O_8$ nanotubes are produced using the optimal parameters of 220 °C-4 h-10 M. Comparing Fig. 3(a) to (d), the compositions of sodium titanates show tiny changes with increasing

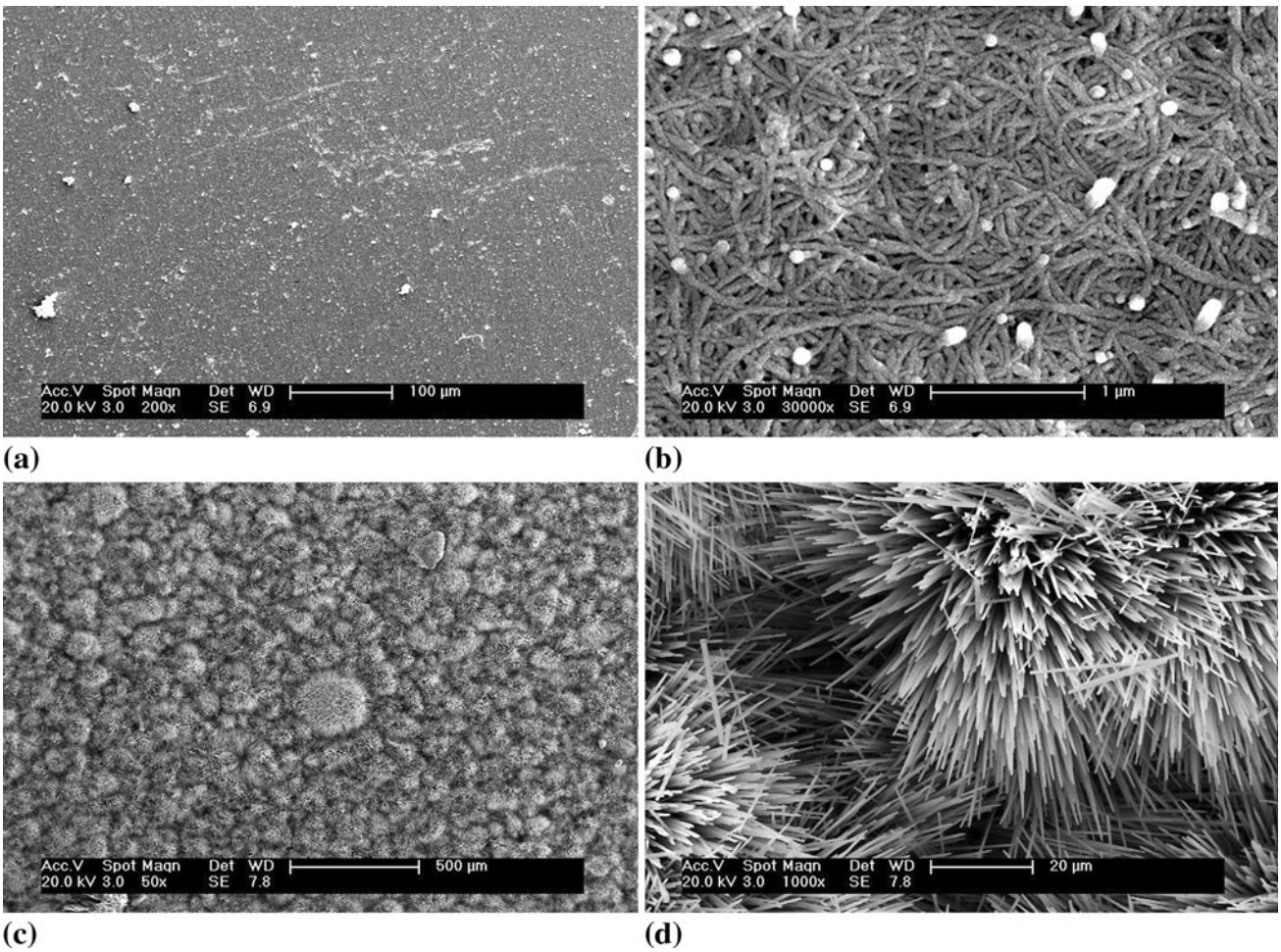

Fig. 2 Morphologies of hydrothermally treated NiTi substrate surface at different temperatures. (a) 150 °C-72 h-10 M; (b) high magnification of (a); (c) 180 °C-72 h-10 M; and (d) high magnification of (c)

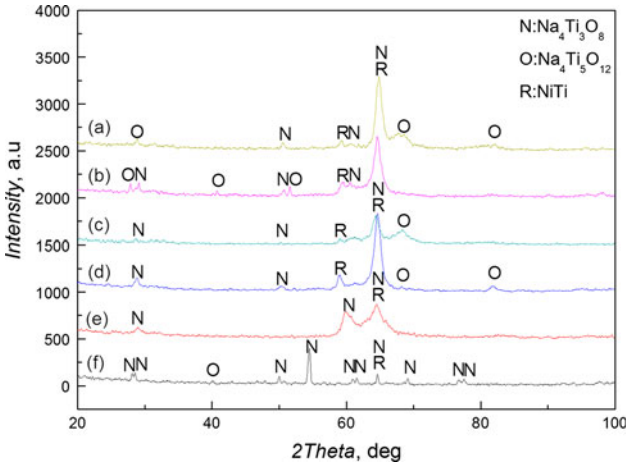

Fig. 3 XRD patterns acquired from hydrothermally treated NiTi under different conditions. (a) 90 °C-6 h-5 M; (b) 120 °C-6 h-10 M; (c) 150 °C-6 h-15 M; (d) 180 °C-6 h-20 M; (e) 150 °C-72 h-10 M; and (f) 180 °C-72 h-10 M

temperature and NaOH concentration for a fixed time duration of 6 h. In contrast, the content of $Na_4Ti_3O_8$ changes as the NiTi diffraction peak decreases from Fig. 3(a) to (b) but increases afterward in Fig. 3(d). When the duration and temperature are increased for a fixed NaOH concentration, the diffraction peaks of $Na_4Ti_3O_8$ change, as shown in Fig. 3(b), (e), and (f). Some peaks of $Na_4Ti_3O_8$ which are present in Fig. 3(f) are completely absent in the other structures are correspond to layered titanates with a monoclinic (*C*2/*m*) lattice, which are also observed when titanate nanotubes transfer into nanoribbon by the other scholar (Ref 25). Meanwhile, the content of NiTi continues to decrease, implying that increasing the temperature and time duration may increase the content of $Na_4Ti_3O_8$ in the range of ~15 M. The reduced NiTi phase leads to diminished Ni release and it is an important criterion for NiTi implants. EDS results show at the early stage of reaction (~6 h) titanate sodium layer is too thin to prevent the exposure of NiTi substrate, which leads to the strong Ni, Ti peaks (Fig. 4a to d). It is because different NaOH concentrations exhibit different reactions efficient in each hydrothermal treatment (Ref 24). The highest Na/Ti atomic ratio 1.03 means the optimal NaOH concentration in this study is 15 M, which is also presented in XRD results as products in this concentration exhibit decrease in NiTi peak compared to Fig. 4(a), (b), and (d). However after 72 h hydrothermal treatment $Na_4Ti_3O_8$ becomes the main hydrothermal product with an atomic ratio Na/Ti $\approx$ 1.3, which is close to atomic ratio of $Na_4Ti_3O_8$.

3.3 Wettability

The contact angles measured on the titanate nanostructures reflect the surface hydrophilicity, as shown in Fig. 5. Our results reveal different degrees of hydrophilicity for samples treated under different conditions. Sodium titanates have recently been reported to be hydrophilic because their unique chemical structures enable easier adhesion of hydroxyl and water (Ref 22). However, XRD shows only small changes in the titanate composition albeit the large variations in the contact angles. Hence, the surface morphology, not chemical structure, plays the more important role in the surface wettability.

4. Discussion

4.1 Formation Mechanism of Titanate Nanostructures

The growth process essentially includes three steps:

1. Transport of growth units from the growth medium.
2. Diffusion and incorporation of growth units on the surface.
3. Advancement of the surface leading to growth.

Therefore, the structures of the surface and growth units are the controlling factors of the morphology of crystal. Here, we particularly focus on the effects of the growth units by using a model of anion coordination-polyhedra, which was first proposed by Zhong (Ref 23, 26, 27). This model hypothesizes that in the crystallization procedure, cations exist in the form of complexes with ligands such as OH^- ions. The growth unit is defined as the complex in which the coordination numbers are equal to that of the formed crystal. In the titanate crystal, the coordination number of Ti is six, and so the growth units of the titanate crystal are $[Ti(OH)_6]^{2-}$ (Fig. 6i). Formation of the growth unit is described in more detail in the following.

First, when the hydrothermal treatment generates a high pressure in the reaction kettle and the concentration of free OH^- in the solution is increased due to the rising temperature. This yields a short distance of supersaturation between the NiTi surface and solution. At the same time, Ti loses electrons near the nucleation sites (Fig. 6iia) and combines with free OH^- forming the structural unit $[Ti(OH)_6]^{2-}$ octahedron on the surface, as shown in Fig. 6(iib) and Eq 1:

$$Ti^{4+} + 6OH^- \rightarrow Ti(OH)_6^{2-} \qquad \text{(Eq 1)}$$

Afterward, in the supersaturated solution, on account of diffusion of ions and deregulation movement among molecules and ions, the structural units $[Ti(OH)_6]^{2-}$ are bonded together forming the cluster $Ti_{m+1}O_{p+3}(OH)_n^{(n+2p-4m+2)-}$, as shown in Fig. 6(iic) and Eq 2. Several $Ti(OH)_6$ combine to form a growth unit with certain dimensions and size.

$$Ti_mO_p(OH)_n^{(n+2p-4m)-}(\text{Crystal}) + Ti(OH)_6^{2-} \rightarrow Ti_{m+1}O_{p+3}(OH)_n^{(n+2p-4m+2)-} + 3H_2O \qquad \text{(Eq 2)}$$

The different connection modes of the same structure of Ti-O octahedrons may produce various shapes on the bottom and form different geometric configurations afterward according to the growth direction. Two parameters, concentration of free OH^- ions and energy stability, strongly influence the formation of the growth units. As described before, supersaturation of free OH^- at the interface is the driving force for the generation of Ti-O octahedrons. The higher NaOH concentration means more free OH^- in the solution and it leads to a higher possibility for Ti^{4+} icons combining with OH^- and generation of structural units on the NiTi surface. Meanwhile, as the structural units are bonded together to form the growth unit, energy is required to stabilize the complex with several Ti-O octahedrons. The calculated results of different connection models (Ref 28) indicate that the requirement for stable energy increases if the number of Ti-O octahedrons is increased or the geometric configurations vary. In the early stage of the hydrothermal reaction, the characteristics of growth units structure control predominantly the morphology of the sodium titanate nanostructures and this is the reason why the titanate

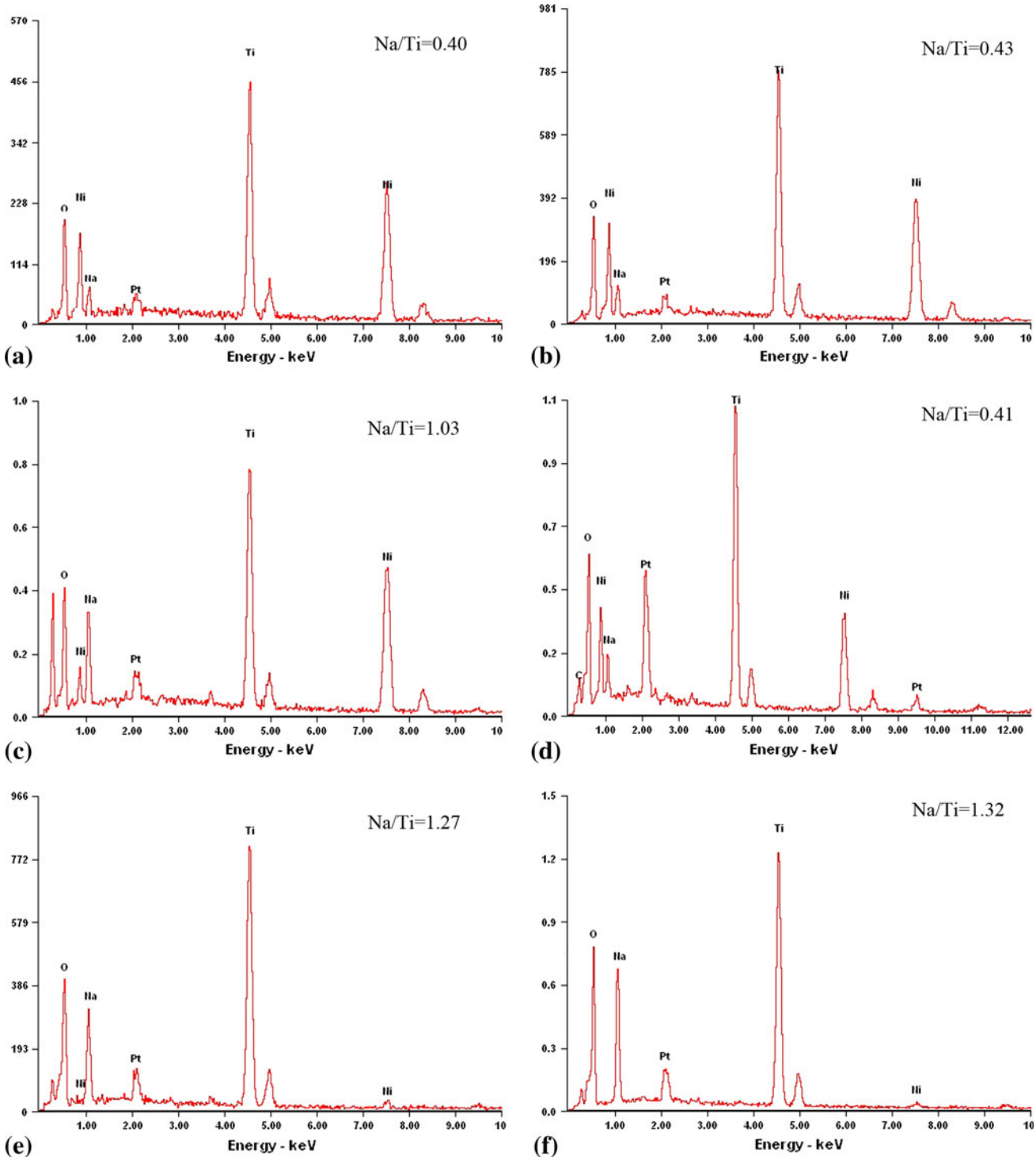

Fig. 4 EDS results acquired from hydrothermally treated NiTi under different conditions. (a) 90 °C-6 h-5 M; (b) 120 °C-6 h-10 M; (c) 150 °C-6 h-15 M; (d) 180 °C-6 h-20 M; (e) 150 °C-72 h-10 M; and (f) 180 °C-72 h-10 M

evolve from one-dimensional nanorods to three-dimensional nanocubes with increasing NaOH concentrations and temperature for a fixed hydrothermal treatment time of 6 h. Nevertheless, the exact procedures are complicated because other reactions occur with time at high temperature. Figure 6 is a schematic illustration of the formation of three typical sodium titanates with a fixed NaOH concentration of 10 M. After combination of the growth units, flake-like structures appear due to the limited NaOH concentration (Fig. 6iid). If the temperature is kept at 120 °C, titanate nanoflakes continue to grow, as shown in Fig. 6(iiia). In contrast, if the temperature is raised, other reactions occur when the time is significantly increased. The unsaturated links at the edge of the titanate flakes give rise to asymmetrical surface tension leading to the conversion into tubular structures (Ref 21, 29). When the temperature is lower, the short tubes continue to grow longer and occasionally asymmetrical tension emerges again causing bending in the long nanofibers (Fig. 6iiib). In another way,

when the temperature is high enough to provide sufficient energy for the short tubes to aggregate (Ref 30), the tubular structures are lengthened and thickened by combining with each other, finally morphing into microscale sea urchin-like microwhiskers, as shown in Fig. 6(iiic).

4.2 Hydrophilicity

The influence of the surface morphology of different sodium titanate nanostructures on wettability can be analyzed by the Wenzel model as follows (Ref 31):

$$\cos\theta_w = r(\sigma_{sv} - \sigma_{sl})/\sigma_{lv} = r\cos\theta_e, \quad \text{(Eq 3)}$$

where θ_w is the apparent contact angle, θ_e is the Eigen contact angle, and σ_{sv}, σ_{sl}, σ_{lv} are the solid-vapor, solid-liquid, liquid-vapor interface tension, respectively.

In this model, the surface roughness positively affects the wettability because the Eigen hydrophilicity of the sodium titanates leads to $\cos\theta_e > 0$ (Ref 32). The surface morphologies are simplified by considering a geometry of square pillars of size $a \times a$, height of H, and spacing of b arranged in a regular array (Ref 33), as shown in Fig. 7. Here, r is defined as the surface roughness factor, as shown in Eq. 4:

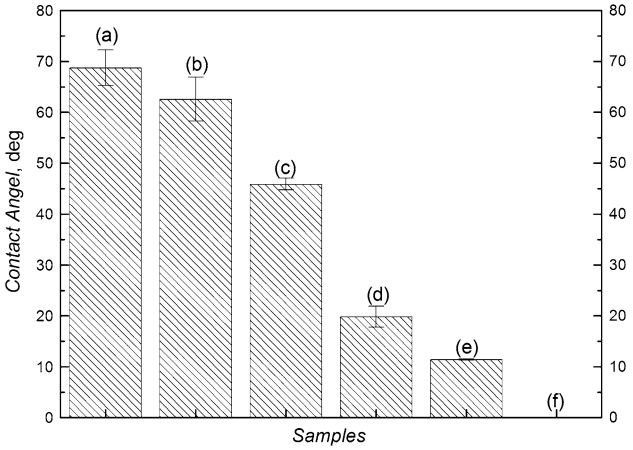

Fig. 5 Hydrophilicity of hydrothermally treated NiTi substrate under different conditions. (a) 180 °C-6 h-20 M; (b) 150 °C-6 h-15 M; (c) 120 °C-6 h-10 M; (d) 90 °C-6 h-5 M; (e) 150 °C-72 h-10 M; and (f) 180 °C-72 h-10 M

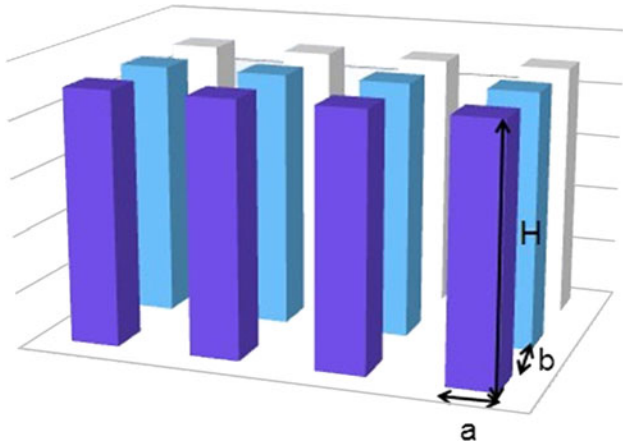

Fig. 7 Simplified NiTi surface by using Wenzel model

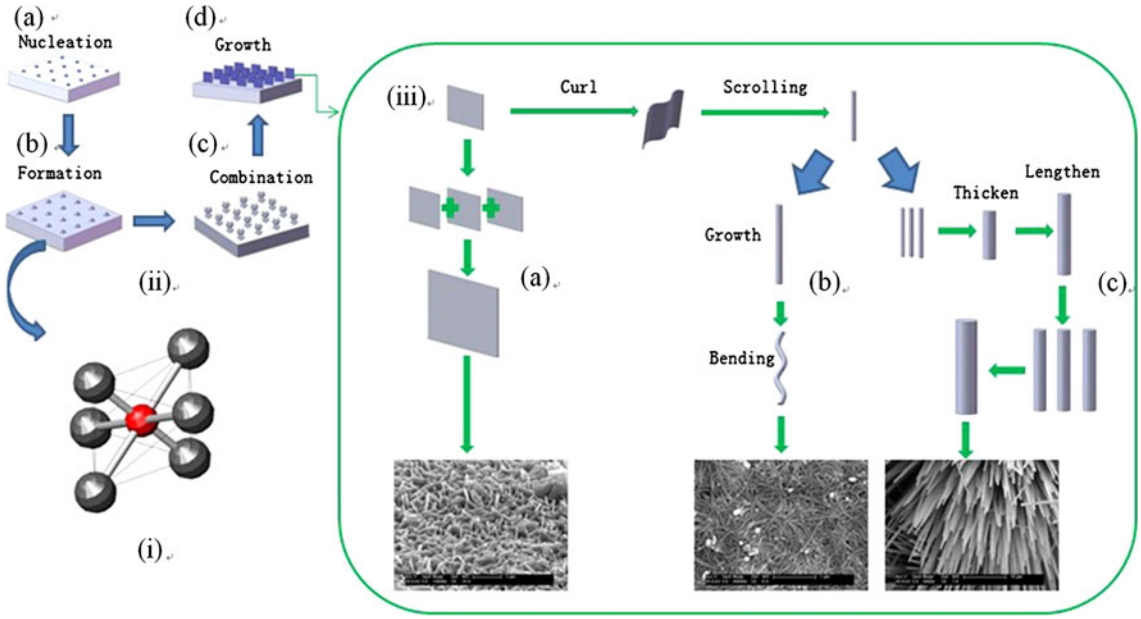

Fig. 6 Schematic diagram depicting the formation of sodium titanate. (i) $[TiO_6]^{8-}$ structural unit; (ii) formation of the growth unit on the substrate: (a) formation of nucleation sites because Ti loses electrons; (b) Ti^{4+} combining with free OH^- to form the structural unit $[Ti(OH)_6]^{2-}$ octahedron on the surface; (c) structural unit $[Ti(OH)_6]^{2-}$ bonded together forming the cluster $Ti_{m+1}O_{p+3}(OH)_n^{(n+2p-4m+2)-}$; (d) appearance of the flake-like structure; (iii) formation of sodium titanate with different morphology: growth process of (a) nanoflakes; (b) nanofibers; (c) microwhiskers

$$r = \frac{(a+b)^2 + 4aH}{(a+b)^2}, \quad \text{(Eq 4)}$$

where $\beta = b/a$ and $\gamma = H/a$. The equation $\cos\theta_w = r\cos\theta_e$ is rewritten as follows:

$$\cos\theta_w = \frac{(a+b)^2 + 4aH}{(a+b)^2}\cos\theta_e = \left[1 + \frac{4\gamma}{(1+\beta)^2}\right]\cos\theta_e. \quad \text{(Eq 5)}$$

As shown in Eq 5, γ and β are the key parameters to control the hydrophilicity on the NiTi surface. The apparent contact angles decrease when the morphology varies due to the increased height/width ratio. This model provides the foundation to control the hydrophilic properties of NiTi SMA.

5. Conclusion

Various types of sodium titanate nanostructures are fabricated on the surface of NiTi SMA under different hydrothermal conditions such as temperature, time duration, and NaOH concentration. XRD spectra disclose that $Na_4Ti_3O_8$ is the major constituent of the reaction product. In the early stage of the hydrothermal treatment, the formation mechanism of titanates is correlated to the free OH^- concentration and energy stabilization. The alkali concentration and hydrothermal temperature affect the shape and size of the titanate nanostructures. As the reaction time is increased, other reactions may lead to the formation of nanorods or even sea urchin-like structure. Controllability of the surface hydrophilicity can be achieved by varying the surface morphology of the sodium titanate nanostructures. For example, increasing the height/width ratio significantly reduces the contact angles.

References

1. T. Duerig, A. Pelton, and D. Stockel, An Overview of Nitinol Medical Applications, *Mater. Sci. Eng. A*, 1999, **273–275**, p 149–160
2. C.L. Chu, R.M. Wang, T. Hu, L.H. Yin, Y.P. Pu, P.H. Lin, S.L. Wu, C.Y. Chung, K.W.K. Yeung, and Paul K. Chu, Surface Structure and Biomedical Properties of Chemically Polished and Electropolished NiTi Shape Memory Alloys, *Mater. Sci. Eng. C*, 2008, **28**, p 1430–1434
3. X. Liu, P.K. Chu, and C. Ding, Surface Nano-Functionalization of Biomaterials, *Mater. Sci. Eng. R*, 2004, **47**, p 49–121
4. S. Shabalovskaya, J. Anderegg, and J. Van Humbeeck, Critical Overview of Nitinol Surfaces and Their Modifications for Medical Applications, *Acta Biomater.*, 2008, **4**, p 447–467
5. E. Conforto, D. Caillard, L. Muller, and F.A. Muller, The Structure of Titanate Nanobelts Used as Seeds for the Nucleation of Hydroxyapatite at the Surface of Titanium Implants, *Acta Biomater.*, 2008, **4**, p 1934–1943
6. M.J. Dalby, N. Gadegaard, R. Tare, A. Andar, M.O. Riehle, P. Herzyk, C.D.W. Wilkinson, and R.O.C. Oreffo, The Control of Human Mesenchymal Cell Differentiation Using Nanoscale Symmetry and Disorder, *Nat. Mater.*, 2007, **6**, p 997–1003
7. M. Karlsson and L. Tang, Surface Morphology and Adsorbed Proteins Affect Phagocyte Responses to Nano-Porous Alumina, *J. Mater. Sci. Mater. Med.*, 2006, **17**, p 1101–1111
8. A.-S. Andersson, J. Brink, U. Lidberg, and D.S. Sutherland, Influence of Systematically Varied Nanoscale Topography on the Morphology of Epithelial Cells, *IEEE Trans. Nanobiosci.*, 2003, **2**(2), p 49–57
9. G. Wei, Q. Jin, W.V. Giannobile, and P.X. Ma, The Enhancement of Osteogenesis by Nano-Fibrous Scaffolds Incorporating rhBMP-7 Nanospheres, *Biomaterials*, 2007, **28**(12), p 2087–2096
10. N. Sugiyama, H. Xu, T. Onoki, Y. Hoshikawa, T. Watanabe, N. Matsushita, X. Wang, F. Qin, M. Fukuhara, M. Tsukamoto, N. Abe, Y. Komizo, A. Inoue, and M. Yoshimura, Bioactive Titanate Nanomesh Layer on the Ti-Based Bulk Metallic Glass by Hydrothermal-Electrochemical Technique, *Acta Biomater.*, 2009, **5**(4), p 1367–1373
11. C.X. Wang, M. Wang, and X. Zhou, Electrochemical Impedance Spectroscopy Study of the Nucleation and Growth of Apatite on Chemically Treated Titanium, *Langmuir*, 2002, **18**, p 7641–7647
12. V. Stengl, S. Bakardjieva, J. Subrt, E. Vecernıkova, L. Szatmary, M. Klementova, and V. Balek, Sodium Titanate Nanorods: Preparation, Microstructure Characterization and Photocatalytic Activity, *Appl. Catal. B*, 2006, **63**, p 20–30
13. H. Zhang, X.P. Gao, G.R. Li, T.Y. Yan, and H.Y. Zhu, Electrochemical Lithium Storage of Sodium Titanate Nanotubes and Nanorods, *Electrochim. Acta*, 2008, **53**, p 7061–7068
14. A. Elsanousi, E.M. Elssfah, J. Zhang, J. Lin, H.S. Song, and C. Tang, Hydrothermal Treatment Duration Effect on the Transformation of Titanate Nanotubes into Nanoribbons, *J. Phys. Chem. C*, 2007, **111**, p 14353–14357
15. R.A. Zarate, S. Fuentes, A.L. Cabrera, and V.M. Fuenzalida, Structural Characterization of Single Crystals of Sodium Titanate Nanowires Prepared by Hydrothermal Process, *J. Cryst. Growth*, 2008, **310**, p 3630–3637
16. H. Yu, J. Yu, B. Cheng, and M. Zhou, Effects of Hydrothermal Post-Treatment on Microstructures and Morphology of Titanate Nanoribbons, *J. Solid State Electron.*, 2006, **179**, p 349–354
17. H.-K. Seoa, G.-S. Kima, S.G. Ansaria, Y.-S. Kima, H.-S. Shina, K.-H. Shimb, and E.-K. Suhb, A Study on the Structure/Phase Transformation of Titanate Nanotubes Synthesized at Various Hydrothermal Temperatures, *Sol Energy Mater Sol C*, 2008, **92**, p 1533–1539
18. X-d Menga, D-z Wang, J-h Liu, and S-y Zhang, Preparation and Characterization of Sodium Titanate Nanowires from Brookite Nanocrystallites, *Mater. Res. Bull.*, 2004, **39**, p 2163–2170
19. H. Zhang, H. Zhao, P. Liu, S. Zhang, and G. Li, Direct Growth of Hierarchically Structured Titanate Nanotube Filtration Membrane for Removal of Waterborne Pathogens, *J. Membr. Sci.*, 2009, **343**, p 212–218
20. M. Ravelingien, S. Mullens, J. Luyten, V. Meynen, E. Vinck, C. Vervaet, and J.P. Remon, Thermal Decomposition of Bioactive Sodium Titanate Surfaces, *Appl. Surf. Sci.*, 2009, **255**, p 9539–9542
21. Y. Guo, N.-H. Lee, H.-J. Oh, C.-R. Yoon, K.-S. Park, S.-C. Jung, and S.-J. Kim, The Growth of Oriented Titanate Nanotube Thin Film on Titanium Metal Flake, *Surf. Coat. Technol.*, 2008, **202**, p 5431–5435
22. S. Wu, X. Liu, T. Hu, P.K. Chu, J.P.Y. Ho, Y.L. Chan, K.W.K. Yeung, C.L. Chu, T.F. Hung, K.F. Huo, C.Y. Chung, W.W. Lu, K.M.C. Cheung, and K.D.K. Luk, A Biomimetic Hierarchical Scaffold: Natural Growth of Nanotitanates on Three-Dimensional Microporous Ti-Based Metals, *Nano Lett.*, 2008, **8**(11), p 3803–3808
23. W.Z. Zhong and S.K. Hua, *Morphology of Crystal Growth*, Science Press, Beijing, 1999
24. Y. Zhang, T. Qi, and Y. Zhang, A Novel Preparation of Titanium Dioxide from Titanium Slag, *Hydrometallurgy*, 2009, **96**, p 52–56
25. D.L. Morgan, H.-Y. Zhu, R.L. Frost, and E.R. Waclawik, Determination of a Morphological Phase Diagram of Titania/Titanate Nanostructures from Alkaline Hydrothermal Treatment of Degussa P25, *Chem. Mater.*, 2008, **20**, p 3800–3802
26. W. Li, E. Shi, W. Zhong, and Z. Yin, Growth Mechanism and Growth Habit of Oxide Crystals, *J. Cryst. Growth*, 1999, **203**, p 186–196
27. C. Xia, E. Shi, W. Zhong, and J. Guo, Hydrothermal Synthesis of $BaTiO_3$ Nano/Microcrystals, *J. Cryst. Growth*, 1996, **166**, p 961–966
28. Y. Zheng, E. Shi, W. Li, Z. Chen, W. Zhong, and X. Hu, The Formation of Titania Polymorphs Under Hydrothermal Condition, *Sci. China E*, 2002, **45**, p 120–129
29. Y.W.L. Lim, Y. Tang, Y.H. Cheng, and Z. Chen, Morphology, Crystal Structure and Adsorption Performance of Hydrothermally Synthesized Titania and Titanate Nanostructures. Nanoscale. doi: 10.1039/c0nr00440e
30. C. Zhang, X. Jiang, B. Tian, X. Wang, X. Zhang, and Z. Du, Modification and Assembly of Titanate Sodium Nanotubes, *Colloids Surf. A*, 2005, **257–258**, p 521–524
31. R.N. Wenzel, Resistance of Solid Surfaces to Wetting by Water, *Ind. Eng. Chem.*, 1936, **28**, p 988–994
32. M. Miyauchi and H. Tokudome, Low-Reflective and Super-Hydrophilic Properties of Titanate or Titania Nanotube Thin Films via Layer-by-Layer Assembly, *Thin Solid Films*, 2006, **515**, p 2091–2096
33. N.A. Patankar, On the Modeling of Hydrophobic Contact Angles on Rough Surfaces, *Langmuir*, 2003, **19**, p 1249–1253